

Article

Microstructure-Tensile Properties Relationship and Austenite Stability of a Nb-Mo Micro-Alloyed Medium-Mn TRIP Steel

Chunquan Liu ^{1,*}, Qichun Peng ^{1,*} , Zhengliang Xue ¹, Mingming Deng ¹, Shijie Wang ¹ and Chengwei Yang ²

¹ The State Key Laboratory of Refractories and Metallurgy, Key Laboratory for Ferrous Metallurgy and Resources Utilization of Ministry of Education, Wuhan University of Science and Technology, Wuhan 430081, China; liuchunquan@wust.edu.cn (C.L.); xuezhengliang@wust.edu.cn (Z.X.); dengmingming1993@163.com (M.D.); wangshijie1994@163.com (S.W.)

² Wuhan Bao Steel Central Research Institute, Wuhan 430083, China; ycw258@baosteel.com

* Correspondence: pengqichun1964@163.com; Tel.: +86-027-8687-0323

Received: 25 June 2018; Accepted: 2 August 2018; Published: 6 August 2018



Abstract: This study investigated the microstructure–tensile properties relationship and the retained austenite room temperature stability of a Nb and Mo micro-alloyed medium manganese transformation induced plasticity (TRIP) steel. A number of findings were obtained. Most importantly, the steel after being processed by quenching and tempering (Q & T) exhibited excellent tensile properties, i.e., the strength of 878–1373 MPa, the ductility of 18–40% Mo, and Nb microalloying served to control the fraction of retained austenite and to improve tensile strength by fine grain strengthening. Excellent tensile properties were attributable to the large amount of retained austenite which produced a discontinuous TRIP effect. This effect led to the production a large amount of martensite which relieved the stress concentration, contributing to the coordinated deformation between the phases and thus improving the deformability of the steel. Additionally, the differences in Mn and C contents led to varying degrees of austenite stability and the length of the Lüders band decreased as the intercritical annealing temperature increased. The micro-alloyed medium manganese steel experimented on our study showed considerable improvement in tensile properties in comparison with the 5Mn-0.1C medium manganese steel in previous studies.

Keywords: medium Mn steel; (Nb; Mo)micro-alloyed; tensile properties; TRIP effect; austenite stability

1. Introduction

Research on automobile plate steel has focused on improving fuel economy and reducing exhaust emissions by lessening vehicle weight in recent years [1]. One plausible strategy to do so is to replace steel with lightweight material such as aluminum alloy, magnesium alloy, composite materials, and carbon fiber [2]. However, those materials are far from ready to substitute steel yet due to numerous problems, including unsatisfactory formation properties, inferior strength and weld ability and, in the case of carbon fiber, the prohibitive cost. As a result, research attention has been shifted to a kind of advanced high-strength steel (AHSS), medium-Mn (4–11%) steel.

As a candidate for automobile plate, medium-Mn steel has such attractive properties as excellent combination of high strength and considerably large ductility (>30 GPa%), light weight, high safety, and relatively lower alloying cost [3–9]. These properties result from the addition of a number of elements featuring Mn. Mn, an austenite stabilizer, triggers an extensive TRIP effect by enhancing the austenite volume fraction, which in turn increases steel strength and ductility. Meanwhile, other

elements may be added to medium-Mn steel to further improve its properties. Among them are Al and C. The addition of 1–3 wt.% Al enhances the kinetics of martensite transformation and promotes precipitation hardening in the martensite matrix [3]. The addition of a trace amount of C (up to ~0.2 wt.%) enhances the kinetics of austenite reversion and austenite stability, and the strength of the alloy [4].

However, these elements can also cause problems. For manganese, most studies added over 5% of this metal to steel. For example, Li et al. [5] reported that hot-rolled 6.1 wt.% Mn steels exhibited superior combination of ultimate tensile strength of 902–1235 MPa and total elongation of 18–42%. Zhao et al. [6] revealed that warm-rolled 7.9 wt.% Mn steels showed superior combination of ultimate tensile strength of 1600 MPa and total elongation of 29%. Cai et al. [7] found that cold-rolled 11 wt.% Mn steel had a tensile strength of 1007 MPa and an overall elongation of 65%. They all added over 5% of manganese because a larger amount of it can better increase austenite stability and stimulate the TRIP effect, thus improving the mechanical properties of the steel. However, high manganese content is prone to segregation, leading to the initiation of brittle cracks [8], and the effect of Mn addition is to decrease the rate of precipitation and the equilibrium precipitate fraction at a given temperature [9]. For this reason, some researchers tried to control manganese below 5%. For example, Merwin [10] reported that cold-rolled 5 wt.% Mn steels achieved a strength–ductility balance exceeding 30 GPa% after the austenite-reverted transformation (ART) heat treatment. Although they succeeded in avoiding the negative effects caused by high manganese content, the medium manganese steel they produced was relatively poor in performance.

A method which can improve steel performance while reducing negative effect is to add trace elements such as Nb and Mo to medium manganese steel. The addition of the microalloying Nb and Mo to medium Mn TRIP steel can increase steel strength because they are conducive for grain refinement, precipitation and solid solution hardening [11]. In addition, they reduce the tendency of Mn and Al to separate during casting and thermoforming [12], and stabilize austenite against transformation to martensite during cooling [13]. Cai et al. [14] experimented adding 0.22 wt.% Mo and 0.05 wt.% Nb to 6.5 wt.% Mn medium Mn steel. The resulting steel exhibited slightly higher ductility and yield strength (YS) values. While their results were satisfactory in terms of ductility and yield strength, their approach could be expensive because of (1) the high prices of manganese, Nb, and Mo, and (2) the complicated processes they adopted.

In this study, we hope to improve steel performance without significantly increasing costs. Accordingly, we investigated the relationship between microstructure and tensile properties of Nb-Mo micro-alloyed 4.73 wt.% Mn steel with an alloy content of no more than 6 wt.% with a much simpler process. Most importantly, we aim to explore the microstructure evolution, mechanical properties, and retained austenite stability in micro-alloyed medium manganese steels. Meanwhile, we also hope to reveal the relationships between deformation behavior and austenite stability, between the effect of temperature on the formation and propagation of Lüders band, and between the discontinuous TRIP effect and the effect of niobium alloying on the microstructure and tensile properties of the experimental steel.

2. Experimental Procedure

The chemical composition of medium manganese steel was 0.12C-4.73Mn-0.82Al-0.19Mo-0.03Nb-Fe (wt.%). A 50 kg vacuum induction melting was used to prepare an experimental steel ingot which was then forged into rods of section size 50 × 30 mm. Afterwards, the ingot was homogenized at 1200 °C for 2 h and hot rolled to 3.6 mm-thick plates via 5 passes between 1150 °C and 850 °C, and subsequently water quenched (WQ) to room temperature (RT). Finally, the steel ingot was cold rolled to 2 mm sheets via 3 passes with the reduction of 44%. The transformation temperatures (A_{C1} of 614 °C, A_{C3} of 765 °C) were calculated using dilatometry. The sample used for dilatometry was a solid cylindrical specimen with a length of 10 mm and a diameter of 3 mm. The dilatometric curve of the experimental steel is shown in Figure 1. The steel sample was heated and kept at a rate of 20 °C/s from room temperature

to 900 °C for thermal expansion for 20 min, and then cooled to the martensite start temperature (Ms) at 100 °C/s. Since long-term intercritical annealing would make austenite too stable to inhibit the TRIP effect [15], the Q&T treatment method for cold rolled strip was adopted. During the Q&T heat treatment process, the experimental steel samples were first annealed at 600 °C, 625 °C, 650 °C, 675 °C, 700 °C, and 750 °C for 30 min respectively, and next WQ to room temperature and then tempered at 200 °C for 15 min (as shown in Figure 2).

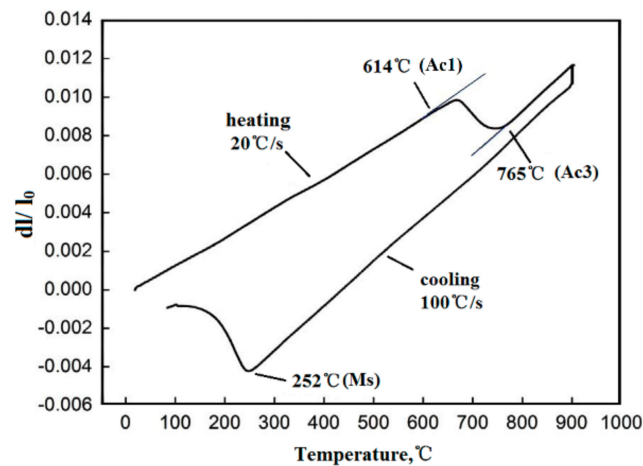


Figure 1. Dilatometric curves for the experimental steel.

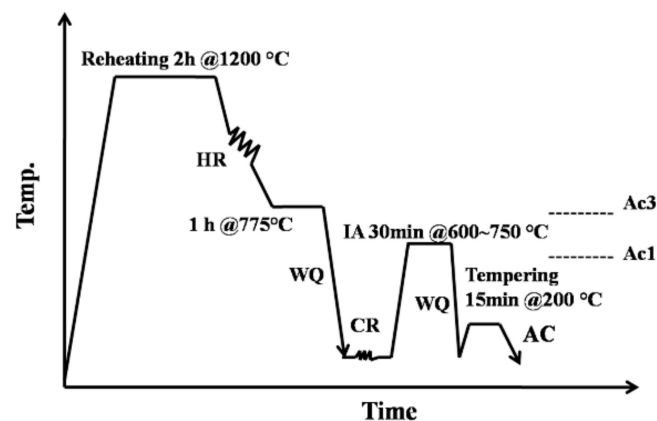


Figure 2. Schematic of the thermo-mechanical treatment for the experimental steel, intercritical annealing temperatures are 600 °C, 625 °C, 650 °C, 675 °C, 700 °C, and 750 °C (HR: hot rolling, CR: cold rolling, AC: air cooling, WQ: water quenching, IA: intercritical annealing).

Tensile specimens were machined to a standard GB/T 228-2010 size of 12.5 mm width and 50 mm gauge length along the rolling direction. The room temperature tensile test was carried out with a constant 3 mm·min⁻¹ cross head speed at the UTM5305 universal tensile test machine (Shenzhen, China). The retained austenite content of the sample was calculated by analyzing the XRD diffraction energy spectrum. The microstructure of the steel was observed by optical microscopy (OM) (Carl Zeiss AG, Jena, Germany), scanning electron microscopy (SEM) (FEI, Hillsboro, OR, USA), and transmission electron microscopy (TEM) (JEOL, Tokyo, Japan). Metallographic specimens were mechanically polished and etched in a 4 vol.% Nital solution and then observed by Zeiss Axio Scope A1 optical micrographs. Secondary electron (SE) imaging was carried out using Nova 400 Nano SEM operated at 10 kV. The SEM samples were treated in the same way as the OM metallographic specimens. TEM was carried out in a JEM 2100 F TEM operated at 200 kV. The volume fraction of

austenite was determined by X-ray diffraction (XRD) using a Bruker X'Pert Pro powder diffractometer (Bruker, Karlsruhe, Germany) with CuK α radiation using direct comparison method [16], using peak search, the diffraction spectrum angle, half width, and integral intensity. The austenite (200), (220), and (311) plane diffraction lines and the diffraction lines of ferrite (200) and (211) planes were selected and used in equation (1) to calculate the retained austenite volume fraction [17].

$$V_{\gamma} = 1.4I_{\gamma}/(I_{\alpha} + 1.4I_{\gamma}) \quad (1)$$

where V_{γ} is the volume fraction of retained austenite, I_{γ} is the integrated intensity of austenite peaks, and I_{α} is the integrated intensity of the ferrite peaks. The contents of C and Mn in austenite at different temperatures were studied using Thermo-Calc (a popular software package for thermo kinetics) combined with TCFE7 database. The phase composition of each temperature in the equilibrium state and the weight percentage of each alloying element in austenite at different temperatures were calculated using Thermo-Calc. 2017b (Thermo-Calc Software, Stockholm, Sweden).

3. Results and Discussion

3.1. Microstructure and Mechanical Properties

The microstructures of the cold-rolled and heat-treated samples are shown in Figure 3. After the addition of Mo, the middle manganese steel increased in hardenability, leading to formation of fine quenched martensite in some austenite grains. The grains gradually refined and banded during annealing at 600–650 °C, with the prior austenite grain boundaries visible (Figure 3a–c). Grain recovery occurred at 675–750 °C in the cold rolled structure as the annealing temperature increased, the martensite plates were completely recovered at 750 °C, and the grains were gradually coarsened with increase in annealing temperature (Figure 3d–f).

The SEM micrographs at annealing temperatures in the range of 600–750 °C are shown in Figure 4. Figure 4a–e describes the microstructure of samples quenched from 600 °C, 625 °C, 650 °C, 675 °C, and 700 °C respectively. The microstructure mainly consisted of a fine ferrite (F) phase and a retained austenite (RA) when the quenching temperature ranged from 600 °C to 700 °C. When the sample was quenched from 750 °C (see Figure 4f), the microstructure of the experimental steel was blocked austenite, ferrite, and martensite. Since blocked austenite was unstable, austenite content dropped to a lower level (see also Figure 6c). As the quenching temperature increased, the austenite grain size increased and the content of C and Mn decreased, resulting in a decrease in austenite stability, rendering austenite more likely transform into martensite. The austenite is significantly reduced due to extensive martensitic (M) transformation. It was noteworthy that the severely deformed microstructure after cold rolling developed into a band-like morphology.

The weight percentages of Mn, C, Al, Mo, and Nb in face centered cubic (FCC) phase, and representation austenite were calculated by Thermo-Calc. (see Figure 5). In the annealing temperature range of 600–750 °C, the Mn content in austenite decreased from 14.4 wt.% to 6.3 wt.% (see Figure 5a). C content in austenite at 625 °C, 650 °C, and 675 °C was 0.394 wt.%, 0.391 wt.%, and 0.343 wt.%, respectively. Thus, compared to C, Mn played a more important role in austenite stability at room temperature. The experimental steel at the annealing temperature of 750 °C resulted in a significant decrease in the thermal stability of austenite due to insufficient Mn enrichment. Simultaneously, the contents of Al and Mo in austenite were in the range of 0.248–0.571 in wt.%, 0.06–0.167 in wt.%, respectively, lower than the nominal chemical composition (see Figure 5b).

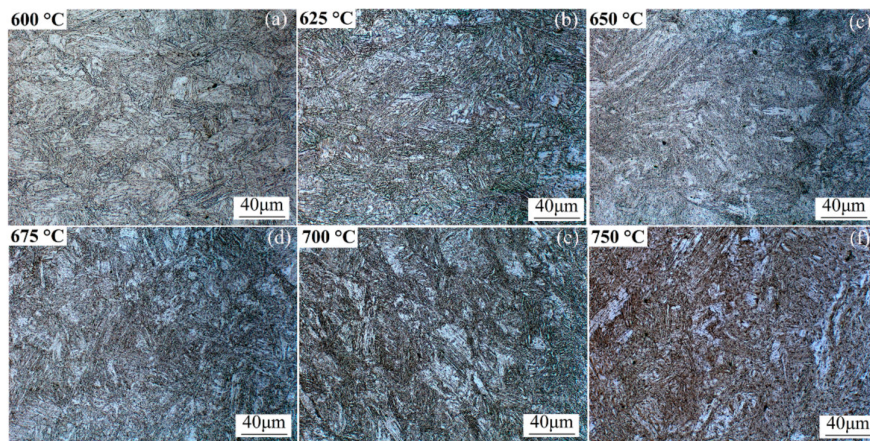


Figure 3. Optical micrographs of experimental steels at different annealing temperatures. (a) 600 °C, (b) 625 °C, (c) 650 °C, (d) 675 °C, (e) 700 °C, and (f) 750 °C.

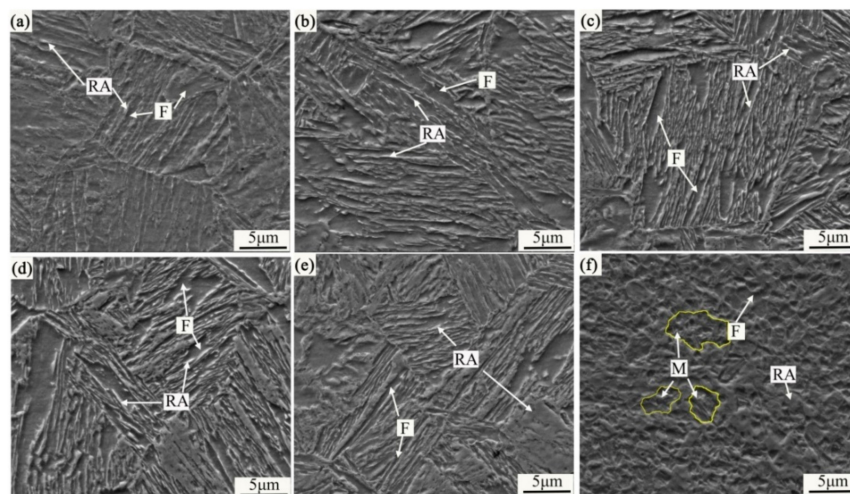


Figure 4. SEM micrographs of experimental steels at different annealing temperatures. (a) 600 °C, (b) 625 °C, (c) 650 °C, (d) 675 °C, (e) 700 °C, and (f) 750 °C (F, ferrite; RA, retained austenite; M, martensite).

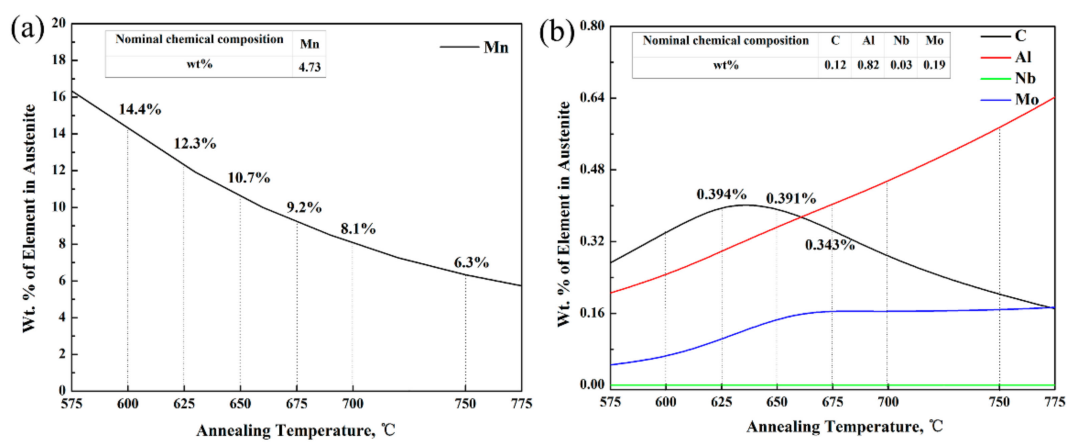


Figure 5. Calculated weight percent of Mn, C, Al, Mo, and Nb in austenite by Thermo-Calc. (a) Mn, (b) C, Al, Mo, and Nb in austenite by Thermo-Calc.

Figure 6 shows the XRD pattern and measured austenite fraction of the experimental steels at different annealing temperatures. The RA fractions of V_γ were calculated using Equation (1) from Figure 6a,b (see Figure 6c). The austenite content in the experimental steel had a maximum of ~39 vol.% at the annealing temperature of 650 °C. As the annealing temperature increased to 750 °C, it decreased to a minimum of ~20 vol.% due to martensite transformation (see also Figure 4f). The transformation ratio of austenite is shown in Figure 6c. The maximum austenite transformation ratio in the experimental steel at an annealing temperature of 650 °C (hence forth referred as the 650 °C sample) was about 87% and the minimum austenite transformation rate in the 750 °C sample was about 55%. The transformation ratio of austenite will be discussed in relation to TRIP effect later.

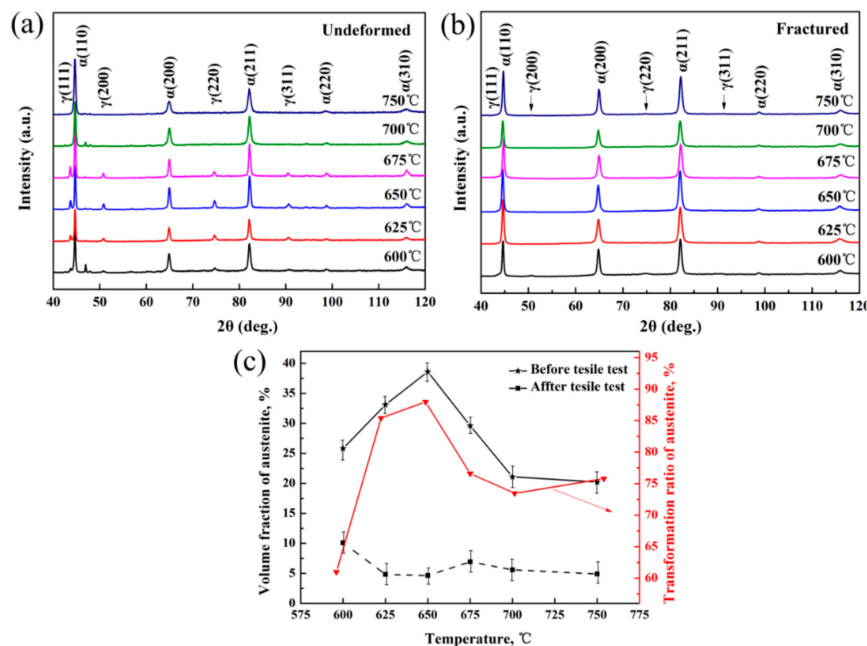


Figure 6. XRD pattern and measured austenite fraction of experimental steels at different annealing temperatures: (a) undeformed, (b) fractured, (c) austenite fraction calculated using Equation (1) and transformation ratio of austenite.

Tensile properties of experimental steels at different annealing temperatures are summarized in Figure 7. The ultimate tensile strength (UTS) reached a maximum value of 1373 MPa as the intercritical annealing temperature increased to 750 °C. Meanwhile, the total elongation (TE) reached a maximum of 40%, with the intercritical annealing temperature rising to 650 °C, and then decreased with a further increase in temperature (see Figure 7b). As shown in Figures 6c and 7b, TE variation remained the same as that of austenite, suggesting that the elongation of experimental steel was closely related to austenite content. The product of ultimate tensile strength and total elongation reached a maximum value of 41.0 GPa% at 650 °C (see Figure 7c). On the other hand, the yield strength reached a minimum of 659 MPa at the annealing temperature of 675 °C. As is shown in Figure 4a–d, the yield strength gradually decreased as the annealing temperature increased from 600 °C to 675 °C due to the softening effect of ferrite phase. In contrast, the hardening effect of the hard phase martensite formed in the material after the annealing temperature was increased from 675 °C to 750 °C, contributing to the rebound of the yield strength. The 650 °C sample, characterized by elongation of 40%, ultimate tensile strength of 1025 MPa, UTS × TE of 41 GPa%, and yield ratio of 0.67 exhibited the best tensile properties which were significantly superior to the values reported for the medium-Mn TRIP steels of a similar chemical composition [18]. The reasons underlying the superior mechanical properties of the sample quenched at 650 °C can be further elucidated by studying austenite stability and its work-hardening behavior.

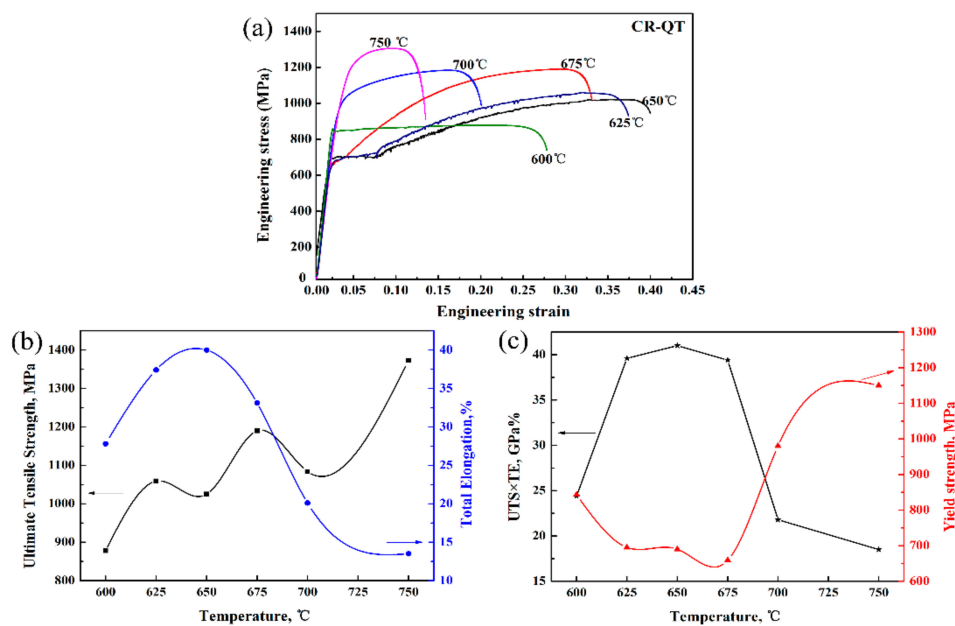


Figure 7. Tensile properties of experimental steels at different annealing temperatures. (a) engineering stress–strain curves, (b) ultimate tensile strength and total elongation and (c) UTS × TE and yield strength. (UTS × TE: product of ultimate tensile strength and total elongation).

3.2. Austenite Stability and Work-Hardening Behaviour

Among the 625 °C, 650 °C, and 675 °C samples, the 650 °C sample contained the largest amount of austenite with 39 vol.%, with 87% transforming to martensite after fracture. In contrast, the 625 °C and 675 °C samples comprised 33.1 and 29.6 vol.% austenite, respectively (Figure 6c), while their austenite transformation rates after fracture were 79% and 84%, respectively. Figure 7b shows that the UTS × TE is closely related to the content of austenite. Retained austenite, the source of the TRIP effect, plays a significant role in the multiphase structure of medium manganese TRIP steel. A prerequisite for this is that the microstructure contained a certain amount of retained austenite with a certain degree of stability. Austenite stability entails thermal stability and mechanical stability. The former is mainly affected by the chemical composition of the material and the heat treatment schedule [19,20] It hinges upon the interplay of internal factors (chemical constituents, austenite grain size, and austenite distribution characteristics, etc.) and external factors (heat treatment schedule, deformation temperature, deformation rate, and stress state, etc.) to result in hysteresis of austenite transformation into martensite. Mechanical stability of austenite is mainly related to deformation temperature, deformation rate, and stress state and can often be calculated by using the following equation [21]:

$$f_{\gamma} = f_{\gamma 0} \exp(-k\varepsilon) \quad (2)$$

In Equation (2), f_{γ} , $f_{\gamma 0}$, and k are austenite fraction at strain ε , initial austenite fraction, and mechanical stability of austenite, respectively. Generally, austenite stability increases as k value decreases [7]. In this study, the k parameter curve of experimental steel samples at different annealing temperatures was 600 °C ($k = 3.4$) < 675 °C ($k = 4.1$) < 625 °C ($k = 5.3$) < 650 °C ($k = 5.4$) < 700 °C ($k = 6.6$) < 750 °C ($k = 10.5$) in descending order (see Figure 8). Admittedly, the tensile properties of the samples did not align well with their k parameter, with 650 °C > 625 °C > 675 °C > 700 °C > 750 °C > 625 °C in descending order (see Figure 8). Most noticeably, the 650 °C sample excelled tensile properties because of its appropriate austenite stability. This is because the largest amount of austenite was produced within the sample at this temperature, a reason also applicable to other samples except the 600 °C one whose excessive austenite stability, as reflected by its k parameter, prevented austenite from

transforming into martensite, ultimately hindering enhancement in tensile properties. These findings suggest tensile properties are closely related to austenite stability regardless of the interference of other factors.

Austenite stability can be reflected via the work-hardening rates (WHR) during the tensile process. The WHR of the three samples with comparatively better tensile properties are presented in Figure 9, with those of the samples of 625 °C and 650 °C rather similar. Austenite in the 650 °C sample with low stability ($k = 5.4$) transformed at a relatively smaller strain ($\epsilon < 0.025$) while the austenite in the 675 °C sample with high stability ($k = 4.1$) transformed at a larger strain ($\epsilon < 0.03$). The majority of austenite was retained after tensile test among the three samples (consistent with Figure 6). These results suggest that the outstanding ductility of the 650 °C sample is primarily associated with the TRIP effect, whereas the ductility of the 675 °C sample is mainly related to ferrite deformation. It is desirable that the microstructure contains more retained austenite with appropriate stability and that austenite-to-martensitic transformation occurs gradually as the strain increases. In this study, the 650 °C sample ($k = 5.4$) had the largest amount of austenite with appropriate stability, thus enjoying the best tensile properties.

The WHR can be divided to four stages (see Figure 9). The WHR decreased rapidly in stage 1 (S1), remained rather stable until its fluctuation in S2, then varied considerably as true strain increased in S3, and finally decreased in a serrated manner in S4. The WHR performance in four stages can be explained by: soft phase ferrite underwent considerable yield deformation in the early stage of plastic deformation (S1) [22,23]; there was a competition between the strength increasing effect caused by the TRIP effect of retained austenite and the softening effect of ferrite deformation (S2) [24]; the progressive TRIP effect of retained austenite caused the strength increasing effect to overcome the softening effect of ferrite deformation (S3) [25–28]; and the austenite TRIP effect was exhausted due to its negation, similar to S1, at the end of the strain (S4). It was noteworthy that the WHR peaks nearly disappeared with serrated behavior in S4. The enhanced TRIP effect could not compensate for the failure of a large plastic deformation within the microstructures, resulting in a reduction in the work-hardening rate [24].

Therefore, we may infer that the relatively poor tensile properties of the 675 °C sample resulted from the fact that the softening effect of ferrite was slightly greater than the hardening contribution of the TRIP effect (see Figure 9c). In contrast, the excellent ductility of the 625 °C and 650 °C samples seemed to be primarily associated with the discontinuous TRIP effect (see Figure 9a,b), with austenite content in the 650 °C sample higher than the 625 °C one. The amount of austenite can directly influence the exertion of TRIP effect, which in turn caused difference in the mechanical properties of the two samples (see also Figure 6c).

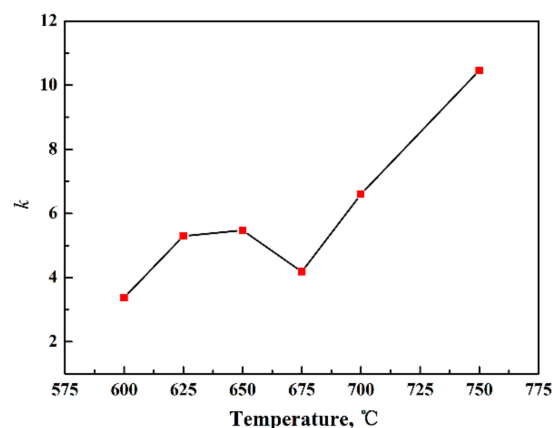


Figure 8. Plots of the k parameter of samples intercritical annealing at different temperatures.

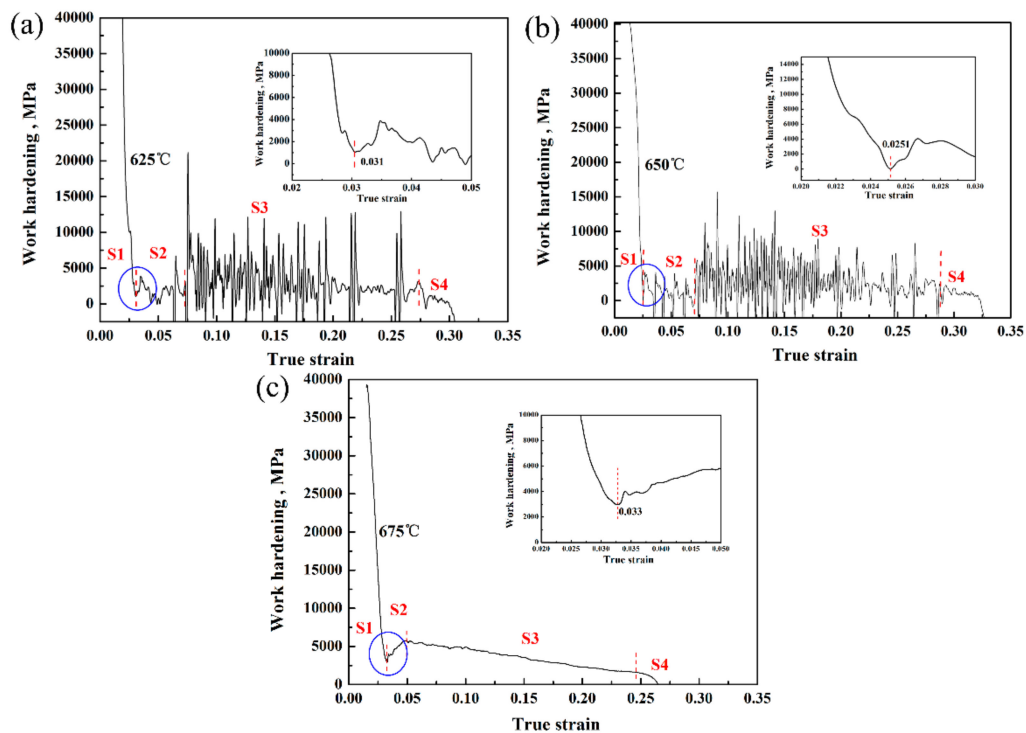


Figure 9. Work-hardening rate of samples at annealing temperatures at (a) 625 °C, (b) 650 °C, and (c) 675 °C.

3.3. Effect of Temperatures on Lüders Bands and Discontinuous TRIP Effect

During the deformation process of the samples, the stress–strain curve of the steel showed two characteristic phenomena, namely the yielding platform and the discontinuous TRIP effect (see Figure 10). The yielding platform phenomenon seemed to be related to Lüders band formation (see Figure 10a). Lüders band formation was generally attributed to the high-density dislocations and explained by Cottrell–Bilby theory [29,30]. It is considered to cause inhomogeneous deformation of local sudden yield of the sheet, resulting in wrinkle bands on the surface of the steel sheet [31]. The length of the Lüders bands at different annealing temperatures is shown in Figure 10a. The Lüders band started from the formation point and then spread out towards the unyielding area of the sample, as shown in the simplified case of 1–3 points. Obviously, the length of Lüders strain decreased as the annealing temperature increased.

WHR fluctuation corresponded to the serrated phenomenon present on the true stress–strain curve, which might be related to the release and concentration of the local stress by the TRIP effect. Figure 10b shows the WHR and the true strain–stress curve of the 650 °C sample. S3 in Figure 10b shows that martensitic transformation was activated when a critical strain of 0.079 was achieved and then transformation occurred continuously in the retained austenite of similar stability with an instantaneous WHR peak 1 (P1). Simultaneously, the corresponding step increase in true stress was obtained. When the strain formed peak points P1 to P2, the true stress gradually increased and the WHR remained almost unchangeable due to the limited or even stoppage of TRIP effect because of the small amount of retained austenite. With further increasing deformation, the accumulated true strain reached another critical strain (0.089), activating partial retained austenite with a relatively high degree of stability to undergo concentrative transformation. Thus, a new round of TRIP effect was initiated, resulting in a new instantaneous WHR peak point, P2, and a substantial increase in true stress.

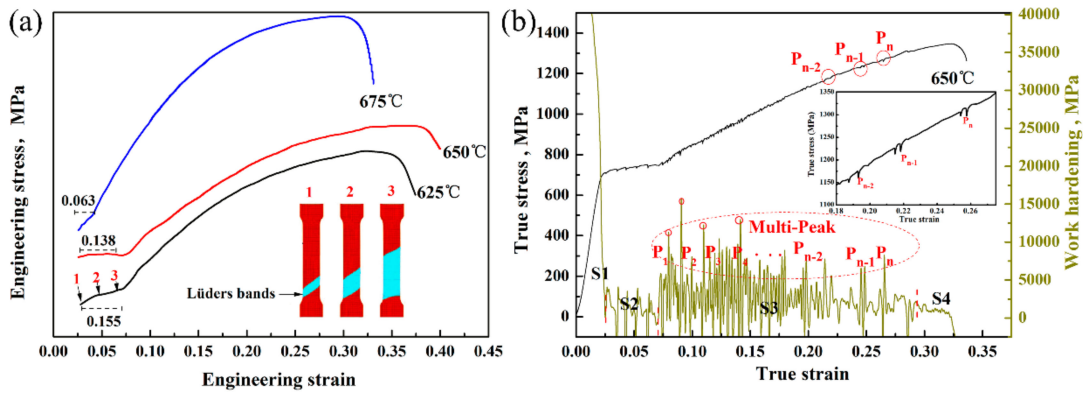


Figure 10. Variation of (a) length of Lüders strain at different temperatures, (b) Work-hardening rate and true strain–stress plot of sample heat treated at 650 °C.

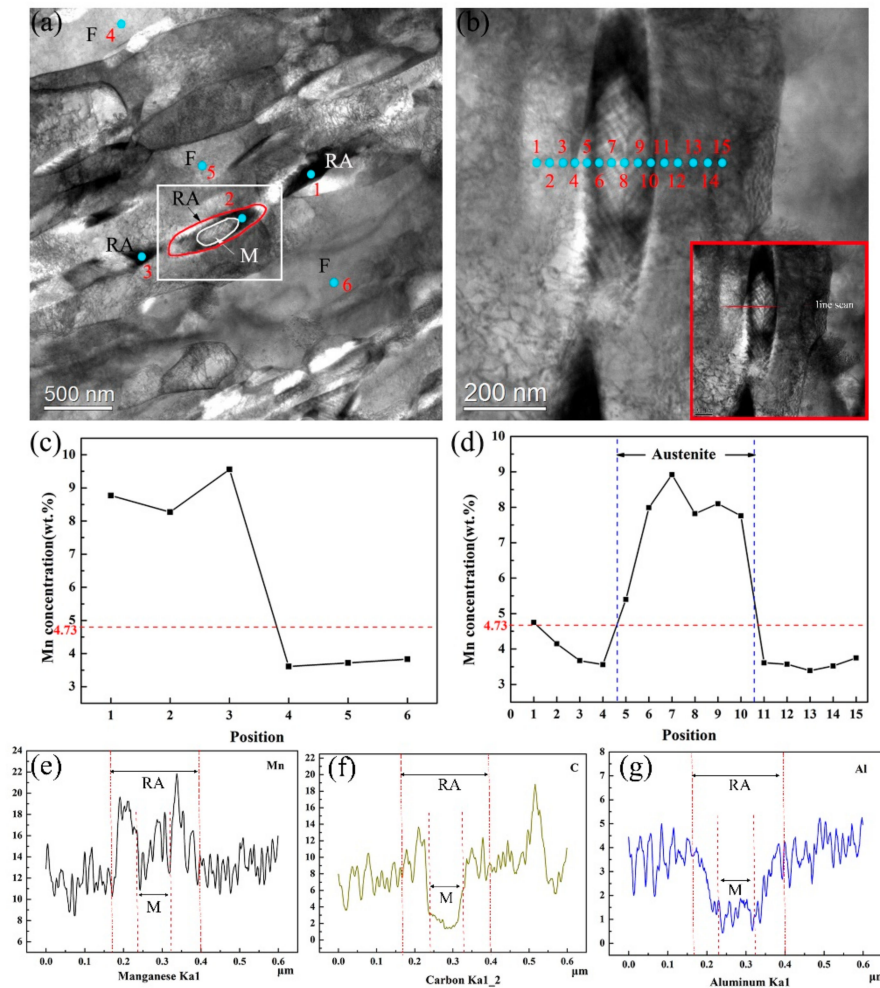


Figure 11. TEM micrograph and EDS analysis showing evidence of Mn partitioned among austenite, ferrite, and martensite: (a) TEM micrograph of the 650 °C sample; (b) TEM micrograph of the area denoted by white square in (a); (c) manganese partitioned in austenite and ferrite of the 650 °C sample in (a); (d) manganese partitioned among austenite, ferrite, and martensite of the 650 °C sample in (b); (e–g) Line scan of the area denoted by red square in (b) for Mn, C, and Al, respectively. F, ferrite; RA, retained austenite; M, martensite; Red coordinates 4.73, the nominal chemical composition of Mn.

Factors significantly affecting austenite stability include chemical composition, heat treatment schedule, distribution characteristics, and so on [19,32–34]. Particularly, the chemical composition has an impressive influence on austenite stability. C and Mn can greatly increase austenite stability at room temperature [20,35]. Mn partitioning among austenite, ferrite, and martensite of the 650 °C sample is shown in Figure 11. Mn distribution appeared higher in austenite grains than in ferrite grains, suggesting that Mn diffused from ferrite to austenite during annealing (see Figure 11a–d). The average Mn content of 12 austenite grains was 8.0 ± 0.3 wt.% and 3.7 ± 0.6 wt.% for 17 ferrite grains; the nominal Mn content in the alloys was 4.73 wt.% and the calculated equilibrium Mn at 650 °C was 10.6 wt.%. The Mn contents in austenite did not reach levels that correspond to full partitioning. These results indicate that the redistribution of Mn during intercritical annealing is not appreciable, probably due to the short annealing time. Furthermore, the Mn content in martensite seemed similar to that in austenite grains (see Figure 11e–g and 11b for Mn, C, and Al, respectively). Mn content in fresh martensite grains was slightly lower than that in retained austenite grains (Figure 11e). In contrast, C and Al contents in fresh martensite grains were significantly lower than those in austenite grains, while Al content in ferrite grains was higher than that in austenite grains (Figure 11f,g). Presumably martensite grains were transformed during quenching from the austenite grains with similar Mn content but lower C content. The effect of chemical composition, particularly carbon and manganese content, can be described in terms of chemical driving force for martensitic transformation in the following equation [36]:

$$\Delta G^{ch} = -7381.6 + 69447X_C + 19296X_{Mn} - 38776X_C X_{Mn} + (6.7821 - 33.45X_C)T \quad (3)$$

ΔG^{ch} is the chemical driving force of martensitic transformation, X_C and X_{Mn} are the mole fraction of carbon and manganese in austenite respectively, and T is the temperature in Kelvin. The chemical driving force of martensitic transformation is shown in Figure 12. The mole fractions of C and Mn were calculated by Thermo-Calc. in combination with TCFE7 database and the chemical driving force of martensite transformation was calculated by Equation (3). Both C and Mn appeared effective stabilizers for austenite with higher C and Mn content contributing together austenite stability. Generally, the content of C in the retained austenite must be controlled within the range of 0.5 wt.%~1.8 wt.%, the higher content of C in retained austenite results in its better stability.

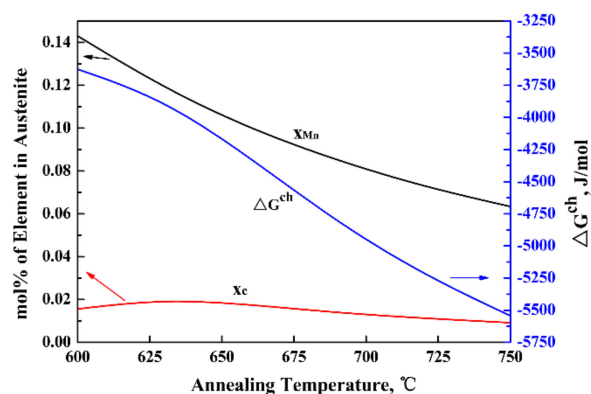


Figure 12. Chemical driving force diagram of martensitic transformation.

3.4. Influence of Nb Alloying On microstructure and Tensile Properties

Figure 13a,c shows the TEM microstructure with NbC precipitates of the 650 °C sample. Certain NbC precipitates in the ferrite grains with grain size of about 36.2 nm (Figure 13b) hindered dislocation movement and played a role in precipitation strengthening. An NbC precipitate in the dislocation line has a pinning effect which hindered dislocation motion during the deformation process [37,38]. This requires more external force to overcome the pinning effect of the deposit

on dislocations and ultimately increases the strength of the matrix by bypassing or shearing the precipitates to generate dislocations. A caveat is in order here. The influence of NbC precipitates of the samples other than the 650 °C one on the mechanical properties of the medium Mn steel requires further study.

Figure 14a schematically shows the evolution of ferrite formation during deformation in the steel without Nb. With the increase of deformation, a large amount of ferrite grains were formed in the austenite grains and grain boundaries, and continuously recrystallized. Figure 14b shows the microstructure evolution of the experimental steel during deformation. At the beginning of deformation, a small amount of film-like ferrite was formed along the austenite grain boundaries. However, as the deformation increased further, the ferrite transformation hardly proceeded. The solute Nb was mainly enriched at ferrite and austenite grain boundaries. The strength-ductility product of the present Mo-Nb micro-alloyed TRIP steel was approximately twice that of the Fe-0.1C-5Mn alloy [39], which was attributable to austenite hardenability, grain refinement, and nanoprecipitation hardening by Nb and Mo additions, in addition to the TRIP effect. The critical driving force for the precipitate of ferrite nucleation given by Equation (4) below was reduced [40]. Thus, the strain-induced driving force for the ferrite formation was consumed by NbC precipitation during the deformation process. Therefore, Nb, having precipitated in the form of NbC particles in the crystal, not only played a role in impeding high-intensity motion of dislocations, but also delayed the transformation of austenite to ferrite due to its segregation effect at the austenite and ferrite grain boundaries. In summary, the Nb contributed to grain refinement and precipitation strengthening.

$$\Delta G_v = \Delta G_{ch} + \Delta G_{st} \quad (4)$$

ΔG_v is the critical driving force for the precipitate of ferrite nucleation, ΔG_{ch} is the chemical driving force of ferrite and ΔG_{st} is the strain-induced driving force of ferrite.

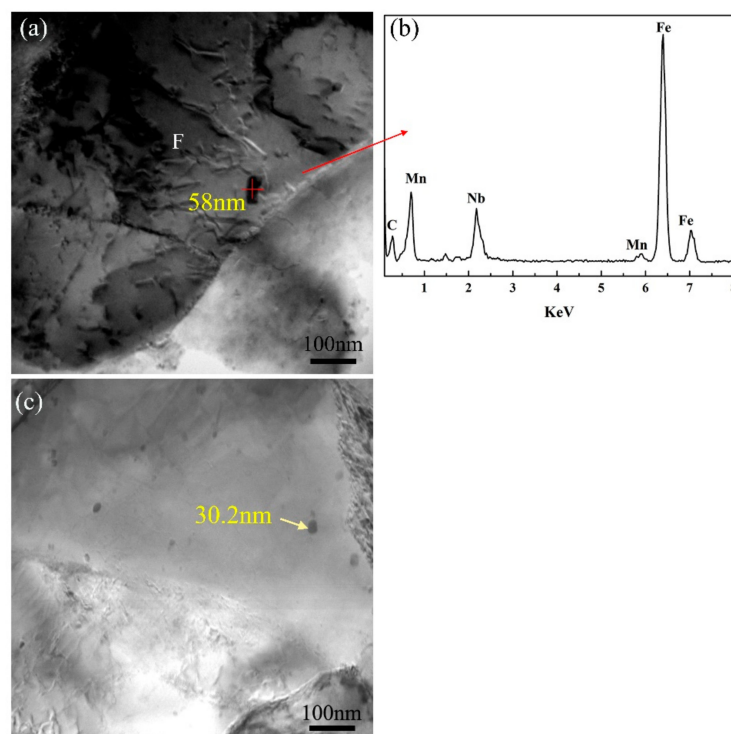


Figure 13. (a) TEM Microstructure of NbC precipitates with grain size of about 58 nm of the 650 °C sample, (b) EDX spectra of NbC precipitates in (a), (c) TEM Microstructure of NbC precipitates with grain size of about 30.2 nm of the 650 °C sample. F, ferrite.

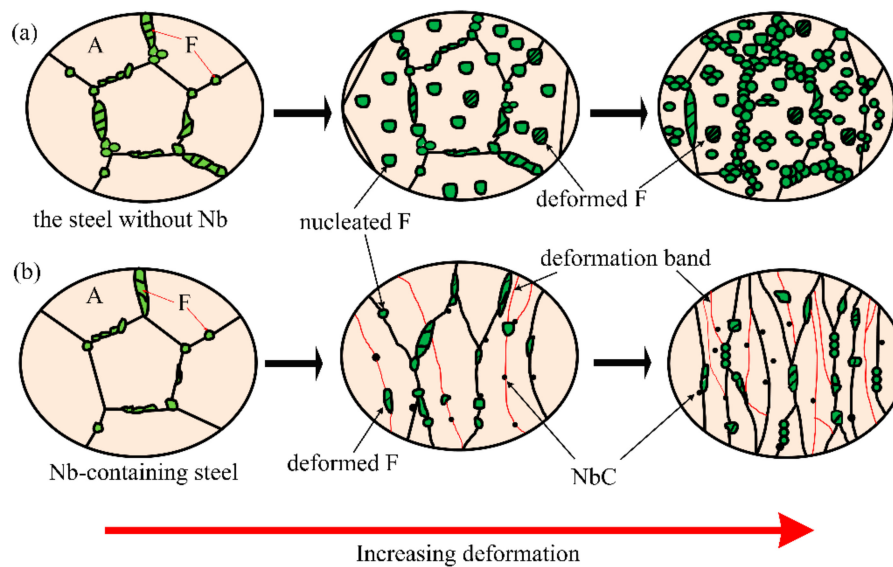


Figure 14. Schematic diagrams of microstructural evolution during deformation. (a) Based on the microstructural evolution data of experimental steel without Nb element in Reference [39]. (b) Nb-containing steel of the 650 °C sample.

4. Conclusions

In this study, we investigated the microstructures, tensile properties, and austenite stability of the Nb and Mo micro-alloyed medium Mn steels with a total alloying addition of less than 6 wt.%. We have come to the following conclusions: (a) The steel subjected to Q & T and quenched from 650 °C for 30 min exhibits the best comprehensive properties with a high volume fraction of austenite (~39%), and is characterized by an excellent combination of TE of 40%, UTS of 1025 MPa, and UTS × TE of 41 GPa%; (b) The optimal mechanical properties of the 650 °C sample are primarily associated with the discontinuous TRIP effect and secondarily with the cooperative softening effect of ferrite deformation. Austenite in the 650 °C sample has appropriate stability for gradual strain-induced austenite-martensite transformation; (c) Lüders strain decreased in length with an increase in the annealing temperature. The higher stability of austenite was attributable to higher C and Mn enrichment; (d) Nb impedes the high intensity motion of dislocations, and delays the transformation of austenite to ferrite while Mo increases the hardenability of experimental steel. The micro-alloyed medium manganese steel experimented in our study showed considerable improvement in tensile properties in comparison with the 5Mn-0.1C medium manganese steel in previous studies.

Author Contributions: Conceptualization, C.L., Q.P., and Z.X.; Methodology, C.L., M.D., S.W., and C.Y.; Writing-Original Draft Preparation, C.L. and Z.X.; Writing-Review & Editing, C.L., M.D., S.W. and C.Y.; Project Administration, Q.P.

Funding: This research received no external funding.

Acknowledgments: We thank Na Luo for her extremely helpful assistance in revising the manuscript. We also thank Hengyang Valin steel Tube Co, Ltd. (HYST) and China Bao Wu Wuhan Iron and Steel Group Co, Ltd. for technical assistance and financial support.

Conflicts of Interest: The authors declare no conflict of interest.

References

1. Pereloma, E.V.; Russell, K.F.; Miller, M.K.; Timokhina, I.B. Effect of pre-straining and bake hardening on the microstructure of thermo mechanically processed CMnSi TRIP steels with and without Nb and Mo additions. *Scr. Mater.* **2008**, *58*, 1078–1081. [[CrossRef](#)]

2. Shi, X.Z. Analysing the application Trend of lightend Material to the Automobile Production. *J. Liaoning Inst. Sci. Technol.* **2009**, *11*, 10–14.
3. Raabe, D.; Ponge, D.; Dmitrieva, O.; Sander, B. Nanoprecipitate-hardened 1.5 GPa steels with unexpected high ductility. *Scr. Mater.* **2009**, *60*, 1141–1144. [[CrossRef](#)]
4. Kuzmina, M.; Ponge, D.; Raabe, D. Grain boundary segregation engineering and austenite reversion turn embrittlement into toughness: Example of a 9 wt.% medium Mn steel. *Acta Mater.* **2015**, *86*, 182–192. [[CrossRef](#)]
5. Li, Z.C.; Ding, H.; Misra, R.D.K.; Cai, Z.H. Microstructure-mechanical property relationship and austenite stability in medium-Mn TRIP steels: The effect of austenite-reverted transformation and quenching-tempering treatments. *Mater. Sci. Eng. A* **2017**, *682*, 211–219. [[CrossRef](#)]
6. Zhao, X.; Shen, Y.; Qiu, L.; Liu, Y.; Sun, X.; Zuo, L. Effects of Intercritical Annealing Temperature on Mechanical Properties of Fe-7.9Mn-0.14Si-0.05Al-0.07C Steel. *Materials* **2014**, *7*, 7891–7906. [[CrossRef](#)] [[PubMed](#)]
7. Cai, Z.H.; Ding, H.; Misra, R.D.K.; Ying, Z.Y. Austenite stability and deformation behavior in a cold-rolled transformation-induced plasticity steel with medium manganese content. *Acta Mater.* **2015**, *84*, 229–236. [[CrossRef](#)]
8. Pereloma, E.; Gazder, A.; Timokhina, I. Retained Austenite: Transformation Induced Plasticity. In *Encyclopedia of Iron, Steel and their Alloys*; Taylor and Francis: New York, NY, USA, 2016; pp. 3088–3103.
9. Zurob, H.S.; Zhu, G.; Subramanian, S.V.; Purdy, G.R.; Hutchinson, C.R.; Brechet, Y. Analysis of the Effect of Mn on the Recrystallization Kinetics of High Nb Steel: An Example of Physically-based Alloy Design. *ISIJ Int.* **2005**, *45*, 713–722. [[CrossRef](#)]
10. Merwin, M. Microstructure and properties of cold rolled and annealed low-carbon manganese TRIP steels. *Iron Steel Technol.* **2008**, *5*, 6–84.
11. Timokhina, I.B.; Miller, M.K.; Pereloma, E.V. Microstructure-Property Relationship in the Thermo mechanically Processed C-Mn-Si-Nb-Al-(Mo) Transformation-Induced Plasticity Steels Before and After Prestraining and Bake Hardening Treatment. *Metall. Mater. Trans. A* **2012**, *43*, 2473–2483. [[CrossRef](#)]
12. Grajcar, A.; Kalinowska-Ozgowicz, E.; Opiela, M.; Grezgorczyk, B. Effects of Mn and Nb on the macro- and micro segregation in high-Mn high-Al content TRIP steels. *Achiev. Mater. Sci. Eng.* **2011**, *49*, 5–14.
13. Akben, M.G.; Bacroix, B.; Jonas, J.J. Effect of vanadium and molybdenum addition on high temperature recovery, recrystallization and precipitation behavior of niobium-based micro-alloyed steels. *Acta Metall.* **1983**, *31*, 161–174. [[CrossRef](#)]
14. Cai, M.; Li, Z.; Chao, Q.; Hodgson, P.D. A Novel Mo and Nb Micro-alloyed Medium Mn TRIP Steel with Maximal Ultimate Strength and Moderate Ductility. *Metall. Mater. Trans. A* **2014**, *45*, 5624–5634. [[CrossRef](#)]
15. Cai, Z.H.; Ding, H.; Xue, X.; Xin, Q.B. Microstructural evolution and mechanical properties of hot-rolled 11% manganese TRIP steel. *Mater. Sci. Eng. A* **2013**, *560*, 388–395. [[CrossRef](#)]
16. Haidemenopoulos, G.N.; Vasilakos, A.N. On the thermodynamic stability of retained austenite in 4340 steel. *J. Alloys Compd.* **1997**, *247*, 128–133. [[CrossRef](#)]
17. Jha, B.K.; Avtar, R.; Dwivedi, V.S. Structure-property correlation in low carbon low alloy high strength wire rods/wire containing retained austenite. *Trans. Indian Inst. Met.* **1996**, *49*, 133–142.
18. Suh, D.W.; Park, S.J.; Lee, T.H.; Oh, C.S.; Kim, S.J. Influence of Al on the Microstructural Evolution and Mechanical Behavior of Low-Carbon, Manganese Transformation-Induced-Plasticity Steel. *Metall. Mater. Trans. A* **2010**, *41*, 397. [[CrossRef](#)]
19. Moor, E.D.; Matlock, D.K.; Speer, J.G.; Merwin, M.J. Austenite stabilization through manganese enrichment. *Scr. Mater.* **2011**, *64*, 185–188. [[CrossRef](#)]
20. Lee, S.; Lee, S.J.; Cooman, B.C.D. Austenite stability of ultrafine-grained transformation-induced plasticity steel with Mn partitioning. *Scr. Mater.* **2011**, *65*, 225–228. [[CrossRef](#)]
21. Sugimoto, K.I.; Kobayashi, M.; Hashimoto, S.I. Ductility and strain-induced transformation in a high-strength transformation-induced plasticity-aided dual-phase steel. *Metall. Trans. A* **1992**, *23*, 3085–3091. [[CrossRef](#)]
22. Lee, C.Y.; Jeong, J.; Han, J.; Lee, S.J.; Lee, S.; Lee, Y.K. Coupled strengthening in a medium manganese lightweight steel with an in homogeneously grained structure of austenite. *Acta Mater.* **2015**, *84*, 1–8. [[CrossRef](#)]
23. Godet, S.; Jacques, P.J. Beneficial influence of an intercritically rolled recovered ferritic matrix on the mechanical properties of TRIP-assisted multiphase steels. *Mater. Sci. Eng. A* **2015**, *645*, 20–27. [[CrossRef](#)]

24. Xu, Y.B.; Zou, Y.; Hu, Z.P.; Han, D.T.; Chen, S.Q.; Misra, R.D.K. Correlation between deformation behavior and austenite characteristics in a Mn-Al type TRIP steel. *Mater. Sci. Eng. A* **2017**, *698*, 126–135. [[CrossRef](#)]
25. Cai, Z.H.; Ding, H.; Misra, R.D.K.; Kong, H. Unique serrated flow dependence of critical stress in a hot-rolled Fe-Mn-Al-C steel. *Scr. Mater.* **2014**, *71*, 5–8. [[CrossRef](#)]
26. Li, Z.C.; Ding, H.; Cai, Z.H. Mechanical properties and austenite stability in hot-rolled 0.2C-1.6/3.2Al-6Mn-Fe TRIP steel. *Mater. Sci. Eng. A* **2015**, *639*, 559–566. [[CrossRef](#)]
27. Li, Z.C.; Ding, H.; Misra, R.D.K.; Cai, Z.H.; Li, H.X. Microstructural evolution and deformation behavior in the Fe-(6,8.5) Mn-3Al-0.2C TRIP steels. *Mater. Sci. Eng. A* **2016**, *672*, 161–169. [[CrossRef](#)]
28. Li, Z.C.; Misra, R.D.K.; Cai, Z.H.; Li, H.X.; Ding, H. Mechanical properties and deformation behavior in hot-rolled 0.2C-1.5/3Al-8.5Mn-Fe TRIP steel: The discontinuous TRIP effect. *Mater. Sci. Eng. A* **2016**, *673*, 63–72. [[CrossRef](#)]
29. Schwab, R.; Ruff, V. On the nature of the yield point phenomenon. *Acta Mater.* **2013**, *61*, 1798–1808. [[CrossRef](#)]
30. Moor, E.D.; Lacroix, S.; Clarke, A.J.; Penning, J.; Speer, J.G. Effect of Retained Austenite Stabilized via, Quench and Partitioning on the Strain Hardening of Martensitic Steels. *Metall. Mater. Trans. A* **2008**, *39*, 2586–2595. [[CrossRef](#)]
31. Kim, J.H.; Park, W.S.; Chun, M.S.; Kim, J.J.; Bae, J.H.; Kim, M.H.; Lee, J.M. Effect of pre-straining on low-temperature mechanical behavior of AISI 304L. *Mater. Sci. Eng. A* **2012**, *543*, 50–57. [[CrossRef](#)]
32. Zou, Y.; Xu, Y.B.; Hu, Z.P.; Gu, X.L.; Peng, F.; Tan, X.D.; Chen, S.Q.; Han, D.T.; Misra, R.D.K.; Wang, G.D. Austenite stability and its effect on the toughness of a high strength ultra-low carbon medium manganese steel plate. *Mater. Sci. Eng. A* **2016**, *675*, 153–163. [[CrossRef](#)]
33. Lee, S.; De Cooman, B.C. On the selection of the optimal intercritical annealing temperature for medium Mn TRIP steel. *Metall. Mater. Trans. A* **2013**, *44*, 5018–5024. [[CrossRef](#)]
34. Jimenez-Melero, E.; Dijk, N.H.V.; Zhao, L.; Sietsma, J.; Offerman, S.E.; Wright, J.P.; Zwaag, S.V.D. Martensitic transformation of individual grains in low-alloyed TRIP steels. *Scr. Mater.* **2007**, *56*, 421–424. [[CrossRef](#)]
35. Wang, J.; Zwaag, S.V.D. Stabilization mechanisms of retained austenite in transformation-induced plasticity steel. *Metall. Mater. Trans. A* **2001**, *32*, 1527–1539. [[CrossRef](#)]
36. Zhang, S.; Findley, K.O. Quantitative assessment of the effects of microstructure on the stability of retained austenite in TRIP steels. *Acta Mater.* **2013**, *61*, 1895–1903. [[CrossRef](#)]
37. Hu, H.J.; Xu, G.; Wang, L.; Xue, Z.L.; Zhang, Y.; Liu, G. The effects of Nb and Mo addition on transformation and properties in low carbon bainitic steels. *Mater. Des.* **2015**, *84*, 95–99. [[CrossRef](#)]
38. Hu, H.J.; Xu, G.; Zhou, M.X.; Yuan, Q. Effect of Mo Content on Microstructure and Property of Low-Carbon Bainitic Steels. *Metals* **2016**, *6*, 173. [[CrossRef](#)]
39. Hu, J.; Cao, W.; Wang, C.; Wang, C.Y.; Dong, H.; Li, J. Phase transformation behavior of cold rolled 0.1C–5Mn steel during heating process studied by differential scanning calorimetry. *Mater. Sci. Eng. A* **2015**, *636*, 108–116. [[CrossRef](#)]
40. Hong, S.C.; Lim, S.H.; Hong, H.S.; Lee, K.J.; Shin, D.H.; Lee, K.S. Effect of Nb on grain growth of ferrite in C-Mn steel during isothermal holding after severe deformation. *Mater. Sci. Eng. A* **2003**, *355*, 241–248. [[CrossRef](#)]

